

# Subaru high resolution spectroscopy of complex metal absorption lines of QSO HS1603+3820<sup>1</sup>

Toru Misawa<sup>2,3</sup>, Toru Yamada<sup>4</sup>, Masahide Takada-Hidai<sup>5</sup>, Yiping Wang<sup>6</sup>, Nobunari Kashikawa<sup>4</sup>, Masanori Iye<sup>4,7</sup>, and Ichi Tanaka<sup>4</sup>

Received \_\_\_\_\_; accepted \_\_\_\_\_

Accepted for publication in the *Astronomical Journal* (AJ)

---

<sup>1</sup>Based on data collected at Subaru Telescope, which is operated by the National Astronomical Observatory of Japan.

<sup>2</sup>Department of Astronomy, School of Science, University of Tokyo, 7-3-1 Hongo, Bunkyo-ku, Tokyo 113-0033, Japan

<sup>3</sup>misawatr@cc.nao.ac.jp

<sup>4</sup>National Astronomical Observatory, 2-21-1 Osawa, Mitaka, Tokyo 181-8588, Japan

<sup>5</sup>Liberal Arts Education Center, Tokai University, 1117 Kitakaname, Hiratsuka, Kanagawa 259-1292, Japan

<sup>6</sup>Purple Mountain Observatory, National Astronomical Observatories, China

<sup>7</sup>Department of Astronomical Science, The Graduate University for Advanced Studies, 2-21-1 Osawa, Mitaka, Tokyo 181-8588, Japan.

## ABSTRACT

We present a high resolution spectrum of the quasar, HS1603+3820 ( $z_{em}=2.542$ ), observed with the High Dispersion Spectrograph (HDS) on Subaru Telescope. This quasar, first discovered in the Hamburg/CfA Quasar Survey, has 11 C IV lines at  $1.96 < z_{abs} < 2.55$ . Our spectrum covers 8 of the 11 C IV lines at  $z_{abs} > 2.29$  and resolves some of them into multiple narrow components with  $b < 25 \text{ km s}^{-1}$  because of the high spectral resolution  $R=45000$ , while other lines show broad profiles ( $b > 65 \text{ km s}^{-1}$ ). We use three properties of C IV lines, specifically, time variability, covering factor, and absorption line profile, to classify them into quasar intrinsic absorption lines (QIALs) and spatially intervening absorption lines (SIALs). The C IV lines at  $2.42 < z_{abs} < 2.45$  are classified as QIALs in spite of their large velocity shifts from the quasar. Perhaps they are produced by gas clouds ejected from the quasar with the velocity of  $v_{ej} = 8000 \text{ km s}^{-1} - 10000 \text{ km s}^{-1}$ . On the other hand, three C IV lines at  $2.48 < z_{abs} < 2.55$  are classified as SIALs, which suggests there exist intervening absorbers near the quasar. We, however, cannot rule out QIALs for the two lines at  $z_{abs} \sim 2.54$  and  $2.55$ , because their velocity shifts,  $430 \text{ km s}^{-1}$  blueward and  $950 \text{ km s}^{-1}$  redward of the quasar, are very small. The C IV line at  $z_{abs} \sim 2.48$  consists of many narrow components, and has also corresponding low-ionization metal lines (Al II, Si II, and Fe II). The velocity distribution of these low-ionization ions is concentrated at the center of the system compared to that of high-ionization C IV ion. Therefore we ascribe this system of absorption lines to an intervening galaxy.

*Subject headings:* quasars: absorption lines — quasars: individual  
(HS1603+3820)

## 1. Introduction

The bright quasar, HS1603+3820 ( $z_{em}=2.542$ ,  $B=15.9$ ), which was first discovered in the Hamburg/CfA Bright Quasar Survey (Hagen et al. 1995; Dobrzycki et al. 1996), has very unique properties, namely the combination of high redshift, large luminosity, and richness of metal absorption lines. In the spectrum of this quasar, 11 C IV absorption lines were detected at  $1.965 < z_{abs} < 2.554$  (Dobrzycki, Engels, & Hagen 1999; hereafter D99). Among the 11 C IV lines, 8 lines are observed at  $2.420 < z_{abs} < 2.554$ , which corresponds to a velocity shift of  $-10600 \text{ km s}^{-1} < \Delta v < +1000 \text{ km s}^{-1}$  from the quasar. The number density of C IV lines with the rest-frame equivalent width of  $W_{rest} \geq 0.15$  is  $N(z) \sim 21$  per unit redshift at  $z_{abs} \sim 2.38$  with  $\Delta z = 0.34$ . If we combine C IV lines that lie within  $1000 \text{ km s}^{-1}$  of each other to produce a so-called Poisson sample (cf. Sargent, Boksenberg, & Steidel 1988),  $N(z)$  becomes  $\sim 12$ , which is significantly larger than the expected average value,  $N(z) = 2.45_{-0.49}^{+0.60}$ , at  $z_{abs} \sim 2.40$  evaluated for C IV lines with  $W_{rest} \geq 0.15 \text{ \AA}$  and  $v_{ej} > 5000 \text{ km s}^{-1}$  in the previous studies (e.g., Sargent et al. 1988; Steidel 1990; Misawa et al. 2002). Such an extreme overdensity of C IV lines inspired us to get a high resolution spectrum of this quasar with Subaru Telescope for a detailed study of the C IV lines.

Absorbers are generally divided into quasar intrinsic absorption lines (QIALs) and spatially intervening absorption lines (SIALs). QIALs are thought to be produced by gas clouds that are intrinsically associated with the nuclear regions of the quasars. On the other hand, SIALs are produced by either intervening galaxies, which are located along the line of sight of the quasars, or the interstellar matter in the quasar host galaxies. It is essential to understand the origins of the absorption lines in order to answer the questions, such as what causes the extremely high number density of C IV lines in the spectrum of HS1603+3820.

To distinguish QIALs from SIALs, we use the seven proper criteria which have been

proposed in the literatures (Barlow & Sargent 1997; Hamann et al. 1997a; and references therein):

- (1) Time variability of equivalent width is sometimes detected in QIALs.
- (2) QIALs are produced by absorbers with high electron space density.
- (3) Absorbers that produce QIALs cover the background the quasar partially.
- (4) Polarization rate in QIALs is larger than that in the continuum.
- (5) QIALs have smoother and broader line profiles than those of SIALs.
- (6) QIALs are produced by high ionized absorbers.
- (7) QIALs are produced by absorbers with high metallicity.

With one or combination of these criteria, for example, Barlow et al. (1992) found that the broad absorption line (BAL) with  $\text{FWHM} \geq 100 \text{ km s}^{-1}$  near the emission redshift of CSO203 is a QIAL, because the line shows time variability. Hamann, Barlow, & Junkkarinen (1997b) also found that the broad C IV doublet even at  $-24000 \text{ km s}^{-1}$  from Q2343+125 show time variability. Barlow & Sargent (1997) and Hamann et al. (1997a) found QIALs by the covering factor analysis in PKS0123+257 and UM675. Goodrich & Miller (1995) used the polarization method to distinguish QIALs from SIALs in PHL5200 and H1413+117.

For HS1603+3820, D99 used only the covering factor analysis with their low resolution spectrum. They applied the method to the broad C IV line at the high ejection velocity end of the C IV complex, and found that it is a QIAL. However, the other lines were not classified, because they have line profiles narrower than the spectral resolution or maybe they are affected by other lines.

In this paper, we present a high resolution ( $R \sim 45000$ ) spectrum of HS1603+3820

obtained with the High Dispersion Spectrograph (HDS; Noguchi et al. 2002) on the Subaru Telescope. The C IV lines are found to have further complex structure, and we classify them into QIALs and SIALs in order to discuss the cause of their large number density. In § 2, we describe the observations and data reduction. In § 3, the properties of C IV systems are examined, and the classification of C IV systems is delineated in § 4. Results and discussion are given in § 5. We present the conclusions and the prospect of the future work in § 6.

## 2. Observation and Data reduction

We carried out spectroscopic observation of the quasar HS1603+3820 ( $\alpha_{2000} = 16^{\text{h}}04^{\text{m}}55^{\text{s}}.4$ ,  $\delta_{2000} = +38^{\circ}12'01''$ ) with HDS on Subaru Telescope on 2002 March 23 (UT).

It has to be noted that the Ly $\alpha$  emission line is affected by complex metal absorption lines, which makes the value of emission-line redshift of the quasar uncertain (D99). D99 suggested the emission redshift as  $z_{em} \sim 2.51$  by estimating a continuum around the Ly $\alpha$  and C IV emission lines, and considering the fact that the redshifts determined from the broad emission lines can be blueshifted by  $\geq 1200 \text{ km s}^{-1}$  with respect to the systemic redshift from the narrow forbidden lines (Espey 1993). If we match the spectrum of the quasar taken by D99 to the SDSS composite spectrum (Vanden Berk et al. 2001) using O I  $\lambda 1304$  + Si II  $\lambda 1307$  and C II  $\lambda 1335$  emission lines, the systemic redshift of the quasar is estimated to be  $z_{em} = 2.542 \pm 0.003$ . Richards et al. (2002a) also showed that quasars with weaker C IV emission lines tend to be large blueshifted in excess of  $2000 \text{ km s}^{-1}$ . Since the C IV emission line of HS1603+3820 is very weak, the systemic redshift of the quasar may be larger than  $z_{em} = 2.51$ . Therefore we assume  $z_{em}$  of the quasar to be 2.542 instead of  $z_{em} = 2.51$  throughout this paper.

HDS has two  $2\text{k} \times 4\text{k}$  CCDs which are the blue and red CCDs. We adopted 2 pixel

binning along the slit, and we used the red grating with a central wavelength of 6450 Å, which covers 5100 Å – 6400 Å on the blue CCD and 6500 Å – 7600 Å on the red CCD. The results discussed in this paper are based on the spectra taken by the blue CCD alone. The slit width of 0".8 provides the spectral resolution of 45000 (6.67 km s<sup>-1</sup>). The weather conditions were very good, and the seeing was ~ 0".5. The S/N ratio of the spectrum with 2700 sec exposure was ~ 40 per pixel around  $\lambda = 5450$  Å.

The data were reduced with the IRAF package in the standard manner. We determined the continuum by fitting the data with a 3rd order cubic spline function. The spectrum has a heavily absorbed region at around 5300 Å – 5350 Å in the 20th echelle order (Figure 1) and it is not straightforward to determine the continuum level there. In such case, we evaluated the continuum profile of the heavily absorbed order  $i$ ,  $q_i(m)$ , by

$$q_i(m) = \frac{\frac{f_i(m)}{f_{i-1}(m)} \times q_{i-1}(m) + \frac{f_i(m)}{f_{i+1}(m)} \times q_{i+1}(m)}{2}, \quad (1)$$

where  $f_{i-1}(m)$ ,  $f_i(m)$ , and  $f_{i+1}(m)$  are the counts at the  $m$ -th pixel of order  $i - 1$ ,  $i$  and  $i + 1$  of the continuum profile fitted for the flat-frame spectrum,  $q_{i-1}(m)$ , and  $q_{i+1}(m)$  are the counts of order  $i - 1$  and  $i + 1$  of the continuum profile fitted for the quasar spectrum. We acquired the normalized  $i$ -th order spectrum by dividing the quasar spectrum of order  $i$  by  $q_i(m)$ . We used order 17 and 23 to produce  $q_{20}(m)$ , because orders 18, 19, 21, 22 are weakly affected by absorption lines. In the middle window of Figure 1, the interpolated continuum of the order 20,  $q_{20}(m)$ , is shown as a dotted line. For confirmation of the validity of this technique, we applied this method to the stellar spectrum that was used to locate the positions and track the shapes of all the echelle orders. The continuum flux of order  $i$  obtained with this interpolation method is only 3.3 % smaller on average than that of directly fitted spectrum. Therefore, we believe this technique is sufficiently useful for our study.

The normalized spectrum of each order is combined to produce the final spectrum

(Figure 2).

### 3. Identification of C IV systems

We used the VPFIT Voigt profile line-fitting software developed by Carswell et al. (Webb 1987; Carswell et al. 1987). D99 detected 11 C IV lines at  $1.96 < z_{abs} < 2.55$ . Our spectrum covers 8 of them in the range at  $2.42 < z_{abs} < 2.55$  and detected absorption lines at the wavelength of all these lines. Thanks to high spectral resolution, some of C IV lines detected in D99 are further resolved into multiple narrow components, resulting in a total 30 C IV components between  $z = 2.42$  and  $2.55$ . Figure 3 shows both the HDS and MMT spectra (D99; taken from the web site, <http://hea-www.harvard.edu/QEDT/Papers/hs1603>). We summarize the results in Table 1. Column (1) and (2) are the metal line identification and ID number. Column (3) and (4) are observed wavelength and redshift. Column (5) gives the velocity difference from  $z_{em}$ , and column (6) is the Doppler parameter,  $b = \sqrt{2}\sigma$  ( $\sigma$  is velocity dispersion). Columns (7) to (10) are covering factor, optical depth at line center, and column densities in the case of the covering factor  $C_f = 1$  and  $C_f < 1$ , which are discussed in § 4 in detail.

For the sake of simplicity, we divided these C IV lines into four systems, System A to System D as shown in Figure 3. The C IV lines in System B and D in D99 are resolved into multiple narrow components with  $b < 25 \text{ km s}^{-1}$  in our spectrum. The line in System C is not resolved but this line has small Doppler value  $b = 11 \text{ km s}^{-1}$ . On the other hand, the five C IV line clustering in System A in D99 are not further resolved into narrow components, despite that three of them have broad line profiles,  $b > 70 \text{ km s}^{-1}$ . Detailed note on each system is described below.

System A ( $2.42 < z_{abs} < 2.45$ ): D99 detected 5 C IV lines in this system at the velocity

shift of  $-10600 \text{ km s}^{-1} < \Delta v < -7800 \text{ km s}^{-1}$  from  $z_{em}$  in their spectrum. We found additional two C IV lines in our spectrum as shown in Figure 4. In addition to these lines, there still remains the broad absorption feature at  $-9300 \text{ km s}^{-1} < \Delta v < -8000 \text{ km s}^{-1}$ . We cannot separate them to fit the Voigt profile individually because they are heavily blended with each other. Five of the seven detected C IV lines ( $z_{abs} = 2.4186, 2.4257, 2.4341, 2.4362, \text{ and } 2.4510$ ) are relatively broad and smooth, and their appearance are quite similar to each other. On the other hand, the line ( $z_{abs} = 2.4366$ ) has relatively narrow line profile. Perhaps it is an independent system of the broad C IV lines. Another interesting result is that Fe II  $\lambda 1608$  at  $z_{abs} = 2.4367$  detected in D99 have disappeared in our spectrum. But this line could be just a glitch because it looks narrower than the resolution of the spectrum in D99.

System B ( $z_{abs}=2.48$ ): This is the strongest C IV line in the MMT spectrum (D99). Our spectrum resolve this line into 18 narrow components with relatively small Doppler parameters of  $4 \leq b \leq 25 \text{ km s}^{-1}$  (Figure 5), and most of them can be explained by thermal broadening. Relatively low-ionization lines such as Si II  $\lambda 1526$ , Al II  $\lambda 1670$ , and, Fe II  $\lambda 1608$  associated with the C IV lines are also detected (Figure 5). The strongest components of the low-ionization lines are observed at the center of this system, while the weak components exist almost symmetrically at both sides of the strongest one.

System C ( $z_{abs}=2.54$ ): This is one of the two systems within  $1000 \text{ km s}^{-1}$  from the quasar. The line itself is narrow and not resolved into multiple components (Figure 6). There are no other significant metal lines at this redshift.

System D ( $z_{abs}=2.55$ ): Another system within  $1000 \text{ km s}^{-1}$  from the quasar, though this system is redshifted from the quasar. This system is resolved into 4 narrow components (Figure 7). The central two components reach almost zero intensity at their bottoms. The system also do not show up in any other metal lines.



#### 4. Classification of C IV lines

We detected as many as 30 C IV, 7 Al II, 8 Si II, and one Fe II lines with velocity difference in the range of  $-10600 \text{ km s}^{-1} < \Delta v < +1000 \text{ km s}^{-1}$  from the quasar. While all the metal lines discovered are, in terms of the velocity difference, relatively close to the quasar, they could be produced by either gas clouds that are intrinsically associated with the quasar or in intervening galaxies. With the HDS spectrum, we examine the line profiles in detail to classify them into QIAL and SIAL. Among the seven criteria to distinguish QIALs from SIALs described in §1, we mainly use the criteria (1), (3) and (5) which can be directly applied to our spectrum.

##### 4.1. Absorption line profile

Absorbers which produce very broad and smooth profiles are expected to be intrinsically associated with the quasar nuclear region. For example, the broad absorption line systems (BALs) with  $b \sim 10^4 \text{ km s}^{-1}$  are considered to be originated in gas motion in broad line region (BLR) of quasars. On the other hand, intervening absorption lines that inherent to cosmologically intervening galaxies have narrow profile with  $b \leq 12 \text{ km s}^{-1}$ , which corresponds to gas temperature,  $T \sim 10^5 \text{ K}$  for C IV ion.

System A has five relatively broad C IV lines ( $b \geq 65 \text{ km s}^{-1}$ ), and all of them have relatively smooth line profiles and are not resolved into narrow components even in our high-resolution spectrum. Their broad line profiles with  $b (= \sqrt{b_T^2 + b_{tur}^2}) \geq 65 \text{ km s}^{-1}$  are not likely to be produced by only thermal broadening,  $b_T$ , because the corresponding temperature is very high,  $T \geq 3 \times 10^6 \text{ K}$ , compared with typical metal line systems. The micro turbulence,  $b_{tur}$ , is expected to contribute to the majority of the Doppler parameter. Therefore the results strongly suggest that these lines are intrinsic ones which occur in the

vicinity of the quasar nucleus although Doppler parameters of them are too small compared with those of BALs.

On the other hand, System B, C, and D consist of only narrow components with  $b \leq 25$  km s<sup>-1</sup> (corresponding temperature is  $T \leq 4.5 \times 10^5$  K for C IV ion) and 65% of them have  $b < 12$  km s<sup>-1</sup>, which imply that these systems can be produced by intervening galaxies. The component at  $z_{abs} = 2.4412$  in System A also have relatively narrow line profile.

#### 4.2. Partial coverage

We evaluate the covering factor,  $C_f$ , which is the line-of-sight coverage fraction of the absorber over the continuum source. Since the components of absorption systems seem to be fully resolved in our spectrum, we can evaluate the covering factors for C IV doublets, using the following equations:

$$C_f = \begin{cases} \frac{R_r^2 - 2R_r + 1}{R_b - 2R_r + 1} & \text{for } R_r > R_b \geq R_r^2 \\ 1 & \text{for } R_b < R_r^2 \\ 1 - R_r & \text{for } R_b \geq R_r \end{cases} \quad (2)$$

where  $R_b$  and  $R_r$  are residual fluxes at the line centers for blue (C IV  $\lambda 1548$ ) and red (C IV  $\lambda 1551$ ) components of the doublet lines on the normalized spectrum (Hamann et al. 1997a; Barlow & Sargent 1997).

We also evaluated optical depth at line center,  $\tau$ , and the total column density,  $\log N$ , for blue component derived by the following equations (Hamann et al. 1997a; Barlow & Sargent 1997; Savage & Sembach 1991; Peterson 1997):

$$\tau = -\ln \left( \frac{R_b - 1 + C_f}{C_f} \right), \quad (3)$$

$$\log N = \log \left( \frac{\tau b}{f \lambda_0} \right) + 14.576, \quad (4)$$

where  $f$  and  $\lambda_0$  are oscillator strength and the resonance wavelength of the absorption line. For some C IV doublets, blue components reach to almost zero flux, and the residual flux is very uncertain. In that case, we assume that  $C_f = 1$ , and evaluate column densities by directly fitting the Voigt profile for them. The  $C_f$ ,  $\tau$ , and  $\log N$  of 30 C IV components are listed in Table 1. For C IV lines with  $C_f < 1$ , we also evaluate  $\log N$  in the case of  $C_f = 1$  for comparison.

For single lines such as Al II, Si II, and Fe II, we evaluated only the lower limits for  $C_f$ , and  $\tau$  by the eqn. (5) and (6),

$$C_f \geq 1 - R_0, \quad (5)$$

$$\tau \geq -\ln R_0. \quad (6)$$

We also evaluated  $\log N$  in the case of  $C_f = 1$  by the eqn (4).

Al II ( $z_{abs} = 2.4785$ ) and Si II ( $z_{abs} = 2.4785$ ) components in System B reach to almost zero flux at the line centers. We assume that  $C_f = 1$  for them, and evaluated column densities by directly fitting the Voigt profile.

For System A, we evaluated these parameters for only two C IV lines ( $z_{abs} = 2.4186$  and 2.4412), because other lines are heavily blended with each other, or with the Si II lines of System B. For the C IV line at  $z_{abs}=2.4186$ , we also evaluated  $1 \sigma$  errors of the parameters measured in the bottom of the line with  $10 \text{ km s}^{-1}$  velocity width, because this line has very broad line profile ( $\text{FWHM} > 150 \text{ km s}^{-1}$ ), and the line center is uncertain.

The C IV line ( $z_{abs} = 2.4186$ ) in System A is likely to be a QIAL, because the line has  $C_f = 0.31$ . On the other hand, the C IV line at  $z_{abs} = 2.4412$  has  $C_f = 0.8$ , although the value has uncertainty because of its blending with broad C IV lines at the same wavelength region. If those broad C IV lines are removed properly from the spectrum, the  $C_f$  of the C IV line tends to increase toward 1.

The result of the covering factor analysis suggests that System B, C and D cover the quasar completely. The mean  $C_f$  values of 18, 1, and 4 C IV components in System B, C and D are almost unity, 0.943, 1.00 and 0.945 respectively, and 56%, 100%, and 50% of C IV components in these systems have  $C_f=1$ . Only the C IV line at  $z_{abs}=2.4803$  in System B has an exceptionally small covering factor,  $C_f=0.277$ . But this value is tentative, because this line is heavily blended with the blue wing of the C IV line at  $z_{abs}=2.4805$ .

### 4.3. Time variability

Time variability can be a powerful tool in identifying QIALs, simply because once the variability is confirmed, the line is most likely to be a QIAL (but QIALs are not always time variable). There were examples that show this method is indeed very valuable. Absorption lines with time variability were found at  $z_{abs}=2.13$  on the spectrum of UM675 (Hamann et al. 1995), and at  $z_{abs}=2.24$  on the spectrum of Q2343+125 (Hamann et al. 1997b). Equivalent widths of these lines varied by a factor of 3 and 4 within 12 and 0.3 years, respectively.

The Fe II  $\lambda 1608$  line at  $z_{abs}=2.4367$  in the System A shows large time variability, though the identification of this line by D99 probably was not very secure. This line was disappeared in our spectrum, despite that it had been strong ( $W_{rest}=0.11 \text{ \AA}$ ) in D99 (it is seen around  $5525 \text{ \AA}$  in the lower window of Figure 3). The quantitative comparison of the equivalent width of the line in our spectrum with that of D99 is not given, because the spectral resolution was not identical. Nonetheless, if the line identified by D99 would be confirmed to be a real Fe II line at  $z_{abs}=2.4367$ , the presence of the time variability is evident and this line is probably associated with the quasar.

## 5. Results and discussion

Here we classify the detected C IV lines into QIALs and SIALs based on the results in the previous section. After that, we consider the origin(s) of the absorption lines and the cause of the large number density of C IV lines in the spectrum of high-redshift luminous quasar HS1603+3820.

### 5.1. Result of classification based on three criteria

#### 5.1.1. System A

In System A, all of five broad C IV lines have similar smooth line profiles and they are detected within  $3000 \text{ km s}^{-1}$  from each other. One of them at  $z_{abs} = 2.4186$  which corresponds to  $\Delta v = -10600 \text{ km s}^{-1}$  from HS1603+3820 is confirmed to have a small covering factor of  $C_f \sim 0.31$ . For this C IV line, FWHM, column density, and covering factor can be properly measured; they are  $190 \text{ km s}^{-1}$ ,  $15.8$ , and  $0.31$ , respectively, and in similar range of values with those of the already confirmed QIALs,  $440 \text{ km s}^{-1}$ ,  $15.2$  and  $0.19$  for a C IV line at  $-24000 \text{ km s}^{-1}$  from Q2343+125 (Hamann et al. 1997b), and  $56 \text{ km s}^{-1}$ ,  $14.1$  and  $0.31$  for a C IV line at  $-1500 \text{ km s}^{-1}$  from UM675 (Hamann et al. 1997a). The other broad lines in System A can not be fitted individually because of line blending. Nonetheless, they are very likely to be QIALs not only because they have lower ejection velocities (nearer to the quasar) than the C IV line at the lowest redshift ( $z_{abs} = 2.4186$ ) but also because they have similar line profiles to the fitted C IV line.

On the other hand, there is at least one narrow C IV line with  $b \sim 16 \text{ km s}^{-1}$  ( $z_{abs} = 2.4412$ ) in the system, and the line is confirmed to have a large covering factor,  $C_f=0.8$ , with the uncertainty by merging with other broad C IV lines. Covering factor of the line is large,  $C_f$  is close to unity, which also supports the idea that the line is a SIAL. If this is

true, the association of the narrow line and the broad lines in System A is just a chance projection.

There are at least two possible origins for absorbers that produce QIALs in System A. First, we consider the possibility that they are in fact similar absorbers that produce much broader lines in the spectra of the so-called broad absorption line (BAL) quasars. BAL absorbers, which produces lines with  $b = 10,000 - 20,000 \text{ km s}^{-1}$  are thought to be at the distance of a few tens of parsec from the continuum source of quasars (cf. Weymann, Turnshek, & Christiansen 1985; Turnshek et al. 1985). Although widths of the C IV lines in System A with  $b = 60 - 120 \text{ km s}^{-1}$  are much smaller than typical BALs, they can be seen in the spectrum of the quasar at a phase in its transition from (to) a quasi-BAL to (from) a standard quasar (Morris et al. 1986; Richards et al. 2002a). When BAL is formed, many narrow components could blend with each other and make broad absorption feature (BAL) as time passes. Or when BAL dies, most of the optically thin gas of BAL absorbers dissipate and only dense cores that produce narrow lines are left. Ganguly, Charlton, & Bond (2001) also offered the sporadic (or quasi-periodic) mass ejection scenario that would have a density structure of the outflowing wind and produce narrow absorption line clustering.

Another candidate is outflowing clouds accelerated with the jets from the central engine of the quasar. In this case, the absorbing gas extends to distances of hundreds of kpcs (Bridle & Perley 1984). According to the small covering factor of the C IV line at  $z_{abs} = 2.4186$ , however, this interpretation is not favorable because it is difficult for the absorbers at the distance of hundreds of kpcs from the quasar to cover the continuum source partially.

Based on these points, the broad C IV lines in System A are probably produced by outflowing absorbers that are very close to the continuum source. On the other hand, the narrow C IV line at  $z_{abs} = 2.4412$  could be a SIAL which is arisen in an intervening absorber,

or a QIAL which is produced by gas cloud outflowing with almost the same velocity as absorbers of the broad lines, though they are at high altitude because its covering factor is close to unity.

Another remarkable point is that Fe II line at  $z_{abs}=2.4367$  in D99 shows the time variability, which suggests the line is a QIAL. However, the relationship between this line and the corresponding C IV line at nearly same redshift is unclear. Identification of the line as Fe II  $\lambda 1608$  in D99 seems to be based on the detection of C IV lines at the same redshift. In our spectrum in which the line is not seen, however, we still have the corresponding C IV line at nearly the same redshift ( $z_{abs} = 2.4366$ ). In fact, the line has relatively narrow line width,  $b = 25.3 \text{ km s}^{-1}$ , which can be interpreted as a SIAL. If this C IV line is a really SIAL, we argue that the identification of the line at  $5525 \text{ \AA}$  as Fe II  $\lambda 1608$  in D99 may be reconsidered while there are other possibilities that (i) there was another C IV system at the same redshift that was disappeared with Fe II or (ii) the C IV line is a QIAL but only Fe II line has been disappeared.

### 5.1.2. System B

All of the C IV components in System B have narrow line profiles, and they have large covering factors. System B is plausibly produced by clumpy gas clouds in an intervening galaxy. The narrow components distribute within  $\pm 250 \text{ km s}^{-1}$ , which can be explained by the bulk motions in the galaxy. The column density distributions of metal lines, C IV, Al II, Si II, and Fe II, are plotted in Figure 8. High-ionization ion (C IV) distributes more or less evenly within  $\pm 250 \text{ km s}^{-1}$  from the center of System B. On the other hand, lines of low-ionization ions (Al II, Si II, and Fe II) with large column density are seen only near the velocity center; this core-halo structure of low and high ionization lines also supports that the lines are arisen in a galaxy. Gas density in halo clouds is so small that they are easily

affected and highly ionized by background UV flux.

### 5.1.3. System C and D

System C and D are detected within  $1000 \text{ km s}^{-1}$  from the quasar redshift. On one hand, the covering factors of the lines in these systems are near unity, which suggests that they are separated from the continuum source far enough to cover the quasar entirely in the direction of line of sight. On the other hand, their small velocity differences of  $430 \text{ km s}^{-1}$  blueward (System C) and  $950 \text{ km s}^{-1}$  redward (System D) from the quasar redshift imply that they could be physically associated to the quasar.

There are at least two interpretations for these systems. First, the lines may be produced by the intervening galaxies in the vicinity of the quasar that moves around the quasar like cluster (group) of galaxies. The velocity differences of the systems from the quasar ( $\Delta v = 430$  and  $950 \text{ km s}^{-1}$ ) are within the typical velocity dispersion in rich clusters ( $\sigma \sim 1000 \text{ km s}^{-1}$ , for nearby richest cluster of galaxies). The large covering factors,  $C_f \sim 1$ , of these systems can be easily produced by such intervening galaxies. Secondary, the lines could be produced by gas clouds intrinsically associated with the quasar, because System C and D do not have low-ionization lines such as Si II, Al II, and Fe II, which suggests they are on high ionized level. The strong UV flux from the quasar can make them highly ionized. In the disk-wind model (Murray et al. 1995, 1998) that has been used to explain BAL quasars, intrinsic gas clouds exist along the wind streamlines from the continuum source to relatively large distance. The simulations by Proga, Stone, & Kallman (2000) show that once outflowing gas clouds reach a high altitude, they return toward the center along the outflowing stream, which can produce not only blueshifted but also redshifted absorption lines relative to the systemic redshift of the quasar simultaneously. Therefore System C is outflowing from the quasar, while System D has already reached at a high altitude and flow



into the central source of the quasar. These systems should be separate far enough from the quasar to cover the quasar entirely.

## 5.2. Origin of C IV line clustering

If Systems C and D are arisen in the galaxies around the quasar, namely they are SIALs, then five of eight C IV lines detected in D99 at  $2.42 < z_{abs} < 2.55$  are QIALs, and three is SIALs. The number density of SIALs per unit redshift is  $N(z) = 8.82$  at  $z_{abs} \sim 2.38$ . On the other hand, if Systems C and D are classified into be QIALs, the corresponding number density is  $N(z) = 2.94$ , which is almost consistent with the expected value,  $N(z) = 2.45_{-0.49}^{+0.60}$ , at  $z_{abs} \sim 2.40$  (Misawa et al. 2002). Therefore the number density excess of C IV absorption lines at  $z_{abs} \sim z_{em}$  in the spectrum of HS1603+3820 may be caused by the number density excess of QIALs.

Foltz et al. (1986) found that the number density of C IV absorption line increases near the emission redshift of the radio-loud quasars with their  $\sim 1 \text{ \AA}$  resolution spectra. We evaluated the number densities of C IV absorption lines for the 5 quasars in Foltz et al.’s sample (Q1256+357, Q1416+067, Q1445+335, Q1634+176, and Q1756+237) that have strong absorption complexes near the quasars. We used the range of spectra between  $z_{15}$  (the redshift  $15000 \text{ km s}^{-1}$  blueward from  $z_{em}$ ) and  $z_{em}$  or  $z_{high}$  (the redshift at which the C IV absorption line of highest- $z$  is detected beyond  $z_{em}$ ) over which the  $4\sigma$  detection limit corresponds to  $W_{rest} = 0.2 \text{ \AA}$ . The mean value of the C IV number density (not a Poisson sample) is  $\overline{N(z)} = 36.2 \pm 10.0$  per redshift at  $z_{abs} \sim 1.65$ . With the  $\sim 1.5 \text{ \AA}$  resolution spectrum of D99, the number density of C IV line for HS1603+3820 is evaluated to be 43.5 between  $z_{15}$  and  $z_{high}$  ( $z_{abs}$  of System D) over which the  $4\sigma$  detection limit is  $W_{rest} = 0.15 \text{ \AA}$ . The  $N(z)$  for HS1603+3820 has a large value about the same as the mean value  $N(z)$  for 6 quasars in Foltz et al. (1986), though the detection limit of equivalent width and

spectrum resolution are slightly different. These number density excess of C IV lines at  $z_{abs} \sim z_{em}$  could be produced by QIALs.

## 6. Conclusions and future work

We have analyzed the C IV absorption line clustering at  $z_{abs} \sim z_{em}$  in the spectrum of HS1603+3820 using Subaru+HDS data. By using three properties of C IV lines, specifically, time variability, covering factor, and absorption line profile, we have confirmed that among four C IV systems one system is almost certainly intrinsic to the quasar, one system is probably arisen in an intervening galaxy. The other two systems at  $z_{abs} \sim z_{em}$  have properties that are consistent with either interpretation. If they are classified into QIALs, the number density of SIALs in the Poisson sample becomes to be almost consistent with the expected value at the similar redshift far from quasars. In Figure 9, we summarize the distributions of four C IV systems in the physical distance from the quasar in the cases that Systems C and D are classified into SIALs and QIALs.

We finally note some future prospects. In the course of this study, we have not applied the time variability analysis to System B, C, and D, because the resolution of our spectrum is different from that of D99. An additional spectrum taken with the same configuration as our spectrum in a few months to years later might enable us to confirm the time variability of these systems. Deep imaging observation with narrow-band filters for detecting Ly $\alpha$  or H $\alpha$  emission lines of galaxies around the quasar will be also useful to understand the true origins of System C and D. If many galaxies are detected around the quasar at the redshift around  $z_{em}$  of the quasar, they support the idea that System C and D are produced by intervening galaxies in the neighbor of the quasar.

We are grateful for all the staffs of the Subaru telescope, which is operated by the

National Astronomical Observatory of Japan. We would like to thank K. Kawabata, S. Kawanomoto, W. Aoki, and N. Suzuki for their advice about data reduction. We also thank R.F. Carswell, J.K. Webb, A.J. Cooke, and M.J. Irwin for their VPFIT software package available in their web site. We wish to thank the anonymous referee for the report to improve the clarity of this presentation.

## REFERENCES

- Barlow, T.A., & Sargent, W.L.W., 1997, *AJ*, 113, 136
- Barlow, T.A., Junkkarinen, V.T., Burbidge, E.M., Weymann, R.J., Morris, S.L., & Korista, K.T., 1992, *ApJ*, 397, 81
- Bridle, A.H., & Perley, R.A., 1984, *Ann. Rev. Astr. Ap.*, 22, 319
- Carswell R.F., Webb J.K., Baldwin J.A., & Atwood B., 1987, *ApJ*, 319, 709
- Dobrzycki, A., Engels, D., Hagen, H.-J., Elvis, M., Huchra, J., & Reimers, D., 1996, *BAAS*, 188.0602
- Dobrzycki, A., Engels, D., & Hagen, H.-J., 1999, *A&A*, 349, L29 (D99)
- Espey, B.R., 1993, *ApJ*, 411, 59
- Foltz, C.B., Weymann, R.J., Peterson, B.M., Sun, L., Malkan, M.A., & Chaffee, Jr. F.H., 1986, *ApJ*, 307, 504
- Ganguly, R., Charlton, J.C., & Bond, N.A., 2001, *ApJ*, 553, L101
- Goodrich, R.W., & Miller, J.S., 1995, *ApJ*, 448, L73
- Hagen, H.-J., Groote, D., Engels, D., & Reimers, D., 1995, *A&AS*, 111, 195
- Hamann, F., Barlow, T.A., & Junkkarinen, V., 1997b, *ApJ*, 478, 87
- Hamann, F., Barlow, T.A., Junkkarinen, V., & Burbidge, E.M., 1997a, *ApJ*, 478, 80
- Hamann, F., Barlow, T.A., Beaver, E.A., Burbidge, E.M., Cohen, R.D., Junkkarinen, V., & Lyons, R., 1995, *ApJ*, 443, 606

- Misawa, T., Tytler, D., Iye, M., Storrie-Lombardi, L.J., Suzuki, N., & Wolfe, A.M., 2002, *AJ*, 123, 1847
- Morris, S.L., Weymann, R.J., Foltz, C.B., Turnshek, D.A., Shectman, S., Price, C., & Boroson, T.A., 1986, *ApJ*, 310, 40
- Murray, N., & Chiang, J., 1998, *ApJ*, 494, 125
- Murray, N., & Chiang, J., 1995, *ApJ*, 454, L105
- Noguchi, K., Aoki, W., Kawanomoto, S., Ando, H., Honda, S., Izumiura, H., Kambe, E., Okita, K., Sadakane, K., Sato, B., Tajitsu, A., Takada-Hidai, M., Tanaka, W., Watanabe, E., and Yoshida, M., 2002, *PASJ*, 54, 6 in press
- Peterson, B.M., 1997, *An Introduction to Active Galactic Nuclei*, Cambridge University Press §12
- Proga, D., Stone, J.M., & Kallman, T.R., 2000, *ApJ*, 543, 686
- Richards, G.T., Gregg, M.D., Becker, R.H., & White, R.L., 2002a, *ApJ*, 567, L13
- Richards, G.T., Vanden Berk, D.E., Reichard, T.A., Hall, P.B., Schneider, D.P., SubbaRao, M., Thakar, A.R., & York, D.G., 2002b, *AJ*, 124, 1
- Sargent, W.L.W., Boksenberg, A., & Steidel, S.S., 1988, *ApJS*, 68, 539
- Steidel, S.S., 1990, *ApJS*, 72, 1
- Savage, B.D., & Sembach, K.R., 1991, *ApJ*, 379, 245
- Turnshek, D.A., Foltz, C.B., Weymann, R.J., Lupie, O.L., McMahon, R.G., & Peterson, B.M., 1985, *ApJ*, 294, L1
- Vanden Berk, D.E., et al., 2001, *AJ*, 122, 549

Webb, J.K., 1987, PhD thesis, Univ. Cambridge

Weymann, R.J., Turnshek, D.A., & Christiansen, W.A., 1985, in *Astrophysics of Active Galaxies and Quasi-Stellar Objects*, ed. J.S. Miller (Mill Valley, Cal.: University Science Books)

Fig. 1.— Spectrum of HS1603+3820 at echelle orders of 17, 20 and 23 before normalization. With order 17 and 23, the continuum function of order 20 is interpolated (dotted line at the middle window).

Fig. 2.— Normalized Spectrum of HS1603 smoothed by 3 pixels. The obvious cosmic rays are chopped. The lower spectrum in each window is the  $1\sigma$  error level.

Fig. 3.— HDS spectrum with  $R=45000$ , compared to MMT spectrum with  $R \sim 3000$  (D99). Four C IV systems are surrounded by dotted lines at both sides. Fe II 1608 line around  $5525 \text{ \AA}$  in MMT spectrum disappears in HDS spectrum.

Fig. 4.— C IV components of System A. Horizontal axis denotes the velocity shift from the quasar and the observed wavelength. Narrow lines at  $-9800 \text{ km s}^{-1} < \Delta v < -9400 \text{ km s}^{-1}$  are Si II 1526 lines of System B. Thick line in the lower right of figure denotes 10 times width of the instrumental profile ( $66.7 \text{ km s}^{-1}$ ).

Fig. 5.— C IV components of System B. Horizontal axis is the velocity shift from the quasar. Vertical dotted lines denote the positions of C IV 1548 components. Thick line in the lower right of Fe II window denotes 10 times width of the instrumental profile ( $66.7 \text{ km s}^{-1}$ ).

Fig. 6.— Same as Figure 5, but for System C.

Fig. 7.— Same as Figure 5, but for System D.

Fig. 8.— Distributions of column density for C IV, Si II, Al II, and Fe II lines in System B. Open triangle, filled triangle, filled circle, and filled star denote C IV, Si II, Al II, and Fe II lines.

Fig. 9.— Cartoons of the structure of absorbers at  $z_{abs} \sim z_{em}$  in the line of sight to the quasar HS1603+3820. (A) and (B) show the distribution of four systems in the physical distance from the quasar in the cases of Systems C and D being classified into SIALs and

QIALs. Positions of System C and D are exchangeable. (C) shows the distribution of the systems in the observed velocity shift from the quasar.



Table 1. List of metal absorption lines

(1)	(2)	(3)	(4)	(5)	(6)	(7)	(8)	(9)	(10)
Line	ID	$\lambda_{obs}$ (Å)	$z_{abs}$	V (km s <sup>-1</sup> )	b (km s <sup>-1</sup> )	$C_f$	$\tau^a$	$C_f = 1$ log N (cm <sup>-2</sup> )	$C_f < 1$ log N (cm <sup>-2</sup> )
System A : $z_{abs} = 2.44$									
C IV $\lambda 1548$	1	5292.7	2.4186	-10634	114.28 ± 1.96	0.31 ± 0.03 <sup>g</sup>	4.32 <sup>+∞</sup> <sub>-2.03</sub> <sup>g</sup>	14.23	14.80 <sup>+∞</sup> <sub>-0.28</sub> <sup>g</sup>
	2	5303.8	2.4257	-10008	77.68 ± 5.59 <sup>f</sup>	...	...	...	...
	3	5316.7	2.4341	-9276	65.19 ± 2.85 <sup>f</sup>	...	...	...	...
	4	5320.0	2.4362	-9092	80.06 ± 1.52 <sup>f</sup>	...	...	...	...
	5	5320.6	2.4366	-9058	25.30 ± 1.16 <sup>f</sup>	...	...	...	...
	6	5327.7	2.4412	-8656	15.68 ± 0.31	0.796	1.912	13.4	13.6
	7	5342.9	2.4510	-7806	74.36 ± 6.06 <sup>f</sup>	...	...	...	...
System B : $z_{abs} = 2.48$									
C IV $\lambda 1548$	1	5381.8	2.4762	-5628	9.62 ± 0.27	1.000	1.169	13.2	...
	2 <sup>b</sup>	5382.2	2.4764	-5608	7.39 ± 0.11	1.000	...	14.0 <sup>d</sup>	...
	3	5382.8	2.4768	-5573	20.42 ± 1.92	1.000	0.607	13.2	...
	4	5383.0	2.4769	-5560	4.62 ± 0.60	1.000	0.702	12.6	...
	5	5383.3	2.4771	-5544	7.57 ± 2.09	1.000	0.328	12.5	...
	6	5383.8	2.4774	-5519	13.49 ± 4.94	0.977	5.653	13.8	14.0
	7 <sup>b</sup>	5383.9	2.4775	-5512	7.76 ± 0.54	1.000	...	14.1 <sup>d</sup>	...
	8	5384.2	2.4777	-5494	8.84 ± 2.62	0.783	0.958	12.9	13.1
	9	5384.5	2.4779	-5477	9.63 ± 0.53	0.985	2.416	13.5	13.5
	10	5385.0	2.4782	-5450	12.37 ± 0.44	1.000	3.258	13.7	...
	11	5385.6	2.4786	-5416	24.03 ± 2.29	0.997	3.128	14.0	14.0
	12	5386.2	2.4790	-5385	10.65 ± 1.25	0.980	4.072	13.7	13.8
	13	5386.4	2.4791	-5373	20.78 ± 3.19	0.985	1.917	13.7	13.7
	14	5387.1	2.4795	-5336	8.48 ± 0.81	1.000	0.645	12.9	...
	15	5387.4	2.4797	-5319	8.57 ± 0.24	1.000	2.870	13.5	...
	16	5388.3	2.4803	-5268	23.13 ± 1.43	0.277 <sup>e</sup>	0.901	12.8	13.5
	17	5388.6	2.4805	-5251	5.47 ± 0.12	0.987	5.931	13.5	13.6
	18	5389.8	2.4813	-5182	14.49 ± 2.02	1.000	0.131	12.4	...

Table 1—Continued

(1)	(2)	(3)	(4)	(5)	(6)	(7)	(8)	(9)	(10)
Line	ID	$\lambda_{obs}$ (Å)	$z_{abs}$	V (km s <sup>-1</sup> )	b (km s <sup>-1</sup> )	$C_f$	$\tau^a$	$C_f = 1$ log $N$ (cm <sup>-2</sup> )	$C_f < 1$ log $N$ (cm <sup>-2</sup> )
Al II $\lambda 1670$	1	5811.2	2.4781	-5458	12.09 ± 0.65	>0.336	>0.410	11.8	...
	2 <sup>c</sup>	5811.9	2.4785	-5422	9.69 ± 0.16	1.000	...	12.9 <sup>d</sup>	...
	3	5813.4	2.4794	-5345	5.25 ± 1.13	>0.140	>0.151	11.0	...
	4	5813.9	2.4797	-5322	6.37 ± 0.44	>0.361	>0.448	11.6	...
	5	5815.2	2.4805	-5251	4.00 ± 0.19	>0.583	>0.875	11.7	...
	6	5816.4	2.4812	-5193	4.54 ± 0.45	>0.373	>0.466	11.4	...
	7	5816.6	2.4813	-5181	7.15 ± 1.34	>0.225	>0.255	11.4	...
Si II $\lambda 1526$	1	5306.3	2.4757	-5670	11.46 ± 0.35	>0.727	>1.298	13.5	...
	2	5307.5	2.4764	-5606	12.22 ± 1.40	>0.296	>0.351	13.0	...
	3	5310.1	2.4781	-5459	11.23 ± 0.51	>0.322	>0.388	13.0	...
	4 <sup>c</sup>	5310.7	2.4785	-5422	10.73 ± 0.14	1.000	...	14.1 <sup>d</sup>	...
	5	5312.5	2.4797	-5322	8.15 ± 0.37	>0.398	>0.507	12.9	...
	6	5313.7	2.4805	-5252	4.93 ± 0.11	>0.803	>1.625	13.2	...
	7	5314.8	2.4812	-5193	5.63 ± 0.31	>0.497	>0.687	12.9	...
	8	5315.1	2.4814	-5174	13.30 ± 0.55	>0.464	>0.623	13.2	...
Fe II $\lambda 1608$	1	5595.1	2.4786	-5422	5.59 ± 0.27	>0.580	>0.868	13.3	...
System C : $z_{abs} = 2.54$									
C IV $\lambda 1548$	1	5475.9	2.5369	-431	11.11 ± 0.19	1.000	0.860	13.1	...
System D : $z_{abs} = 2.55$									
C IV $\lambda 1548$	1	5500.2	2.5526	+896	9.40 ± 0.51	0.787	0.864	12.9	13.0
	2	5500.5	2.5528	+914	7.64 ± 1.49	1.000	0.297	12.5	...
	3	5500.9	2.5531	+939	12.48 ± 0.30	0.991	6.813	13.9	14.0
	4 <sup>b</sup>	5501.5	2.5535	+970	10.14 ± 0.15	1.000	...	14.6 <sup>d</sup>	...

<sup>a</sup>Optical depth: For C IV line, it is evaluated for bluer component in the case  $C_f$  is the value of column (7). For single line, it is evaluated in the case of  $C_f=1.0$ .

<sup>b</sup>Center of blue component reaches to almost zero flux.

<sup>c</sup>Center of line reaches to almost zero flux.

<sup>d</sup>It is evaluated by fitting the Voigt profile directly.

<sup>e</sup>This line is blended with the blue wing of C IV line at  $z_{abs}=2.4805$ .

<sup>f</sup>It is evaluated for blue component.

<sup>g</sup>One sigma error is evaluated with 10 km s<sup>-1</sup> velocity width, because line profile is very broad and line center is uncertain.

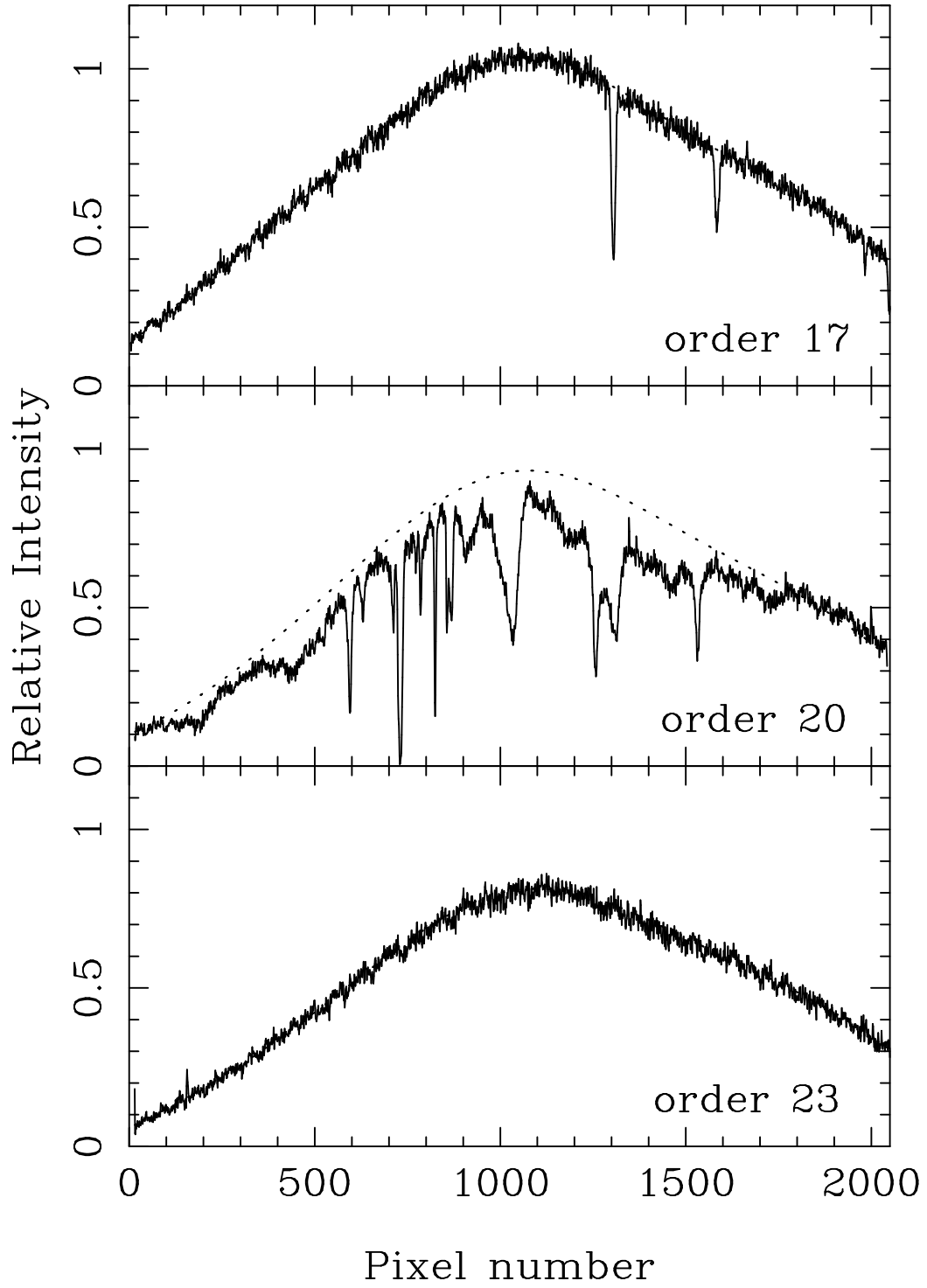


Fig. 1

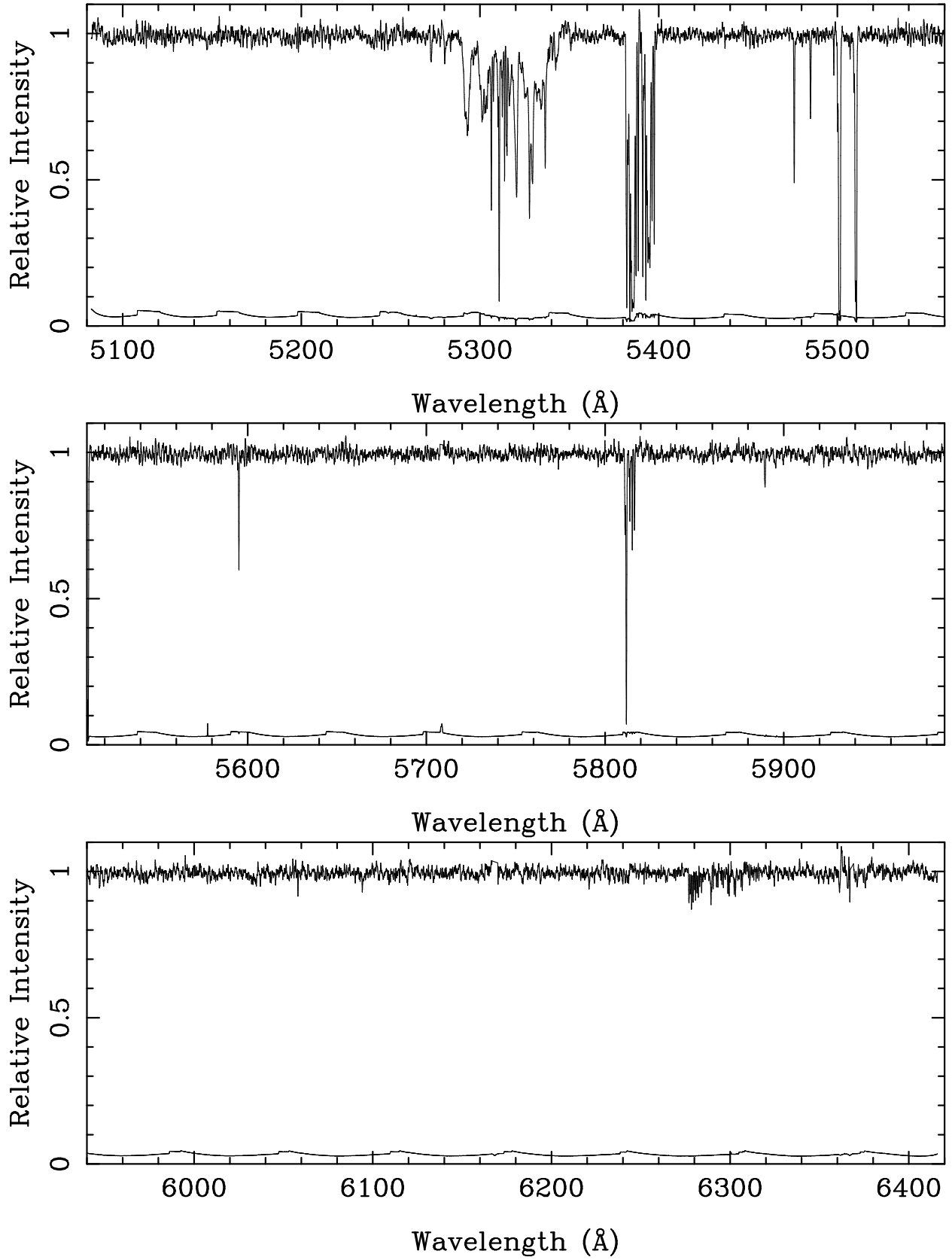


Fig. 2

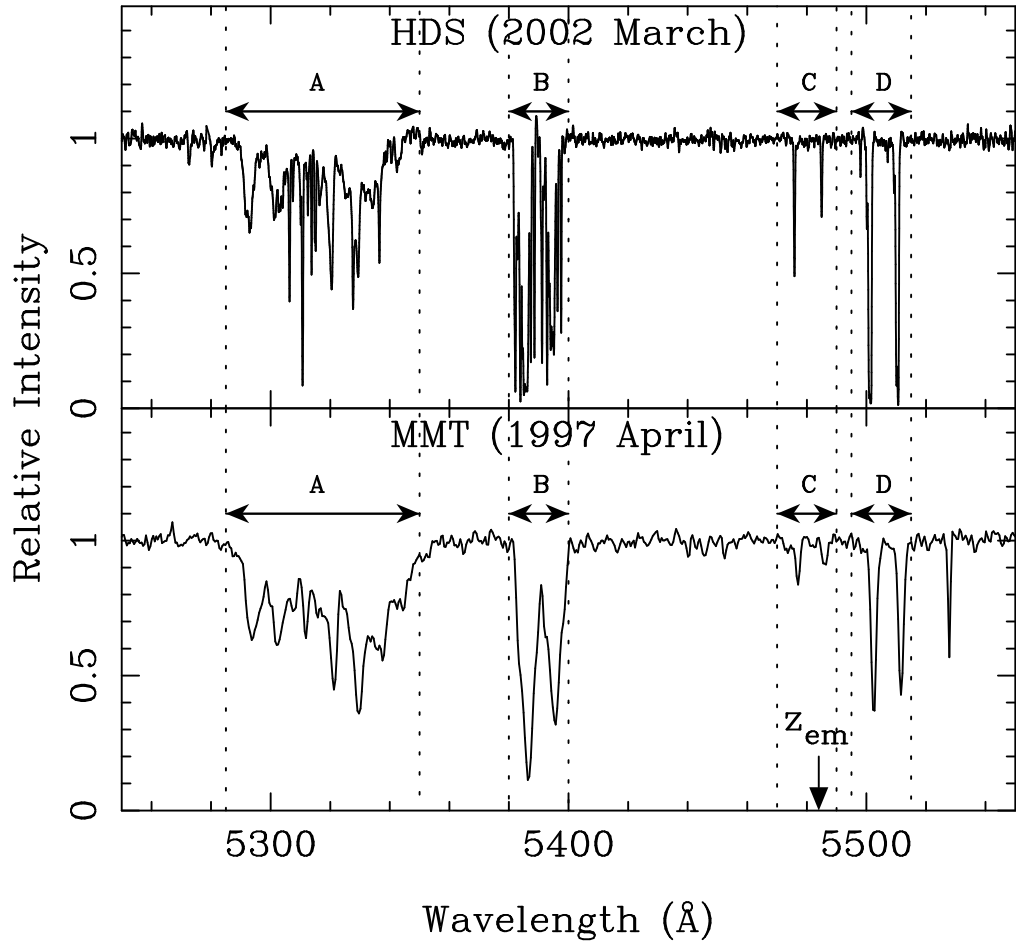
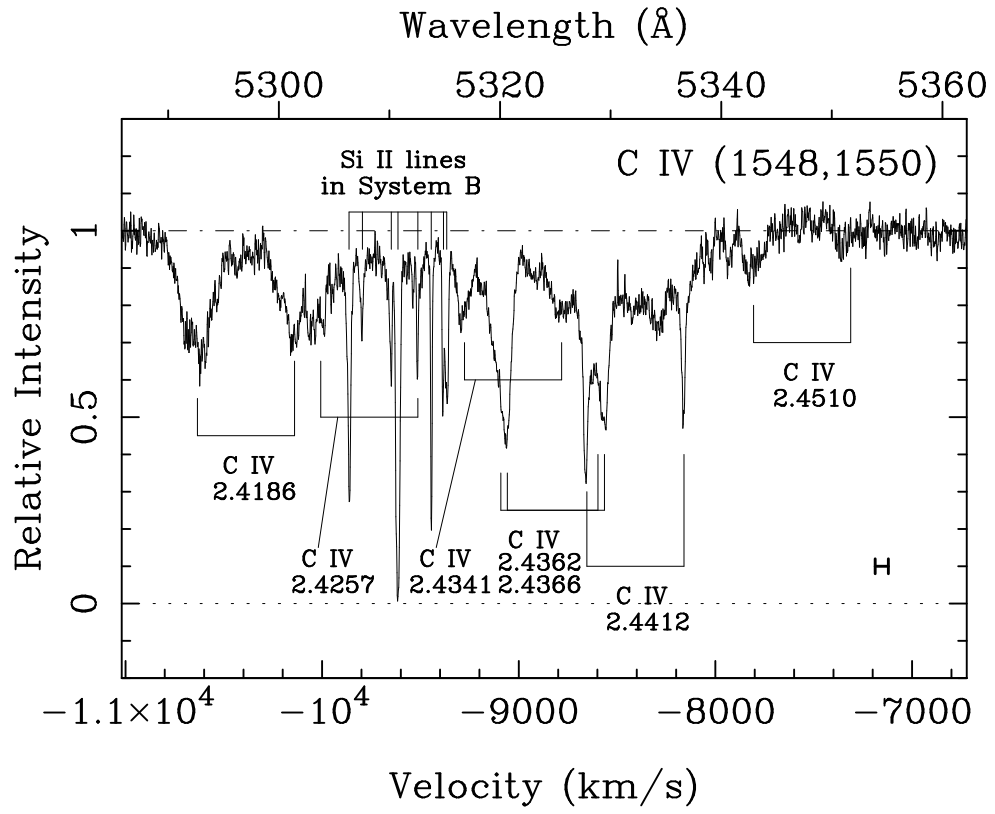


Fig. 3



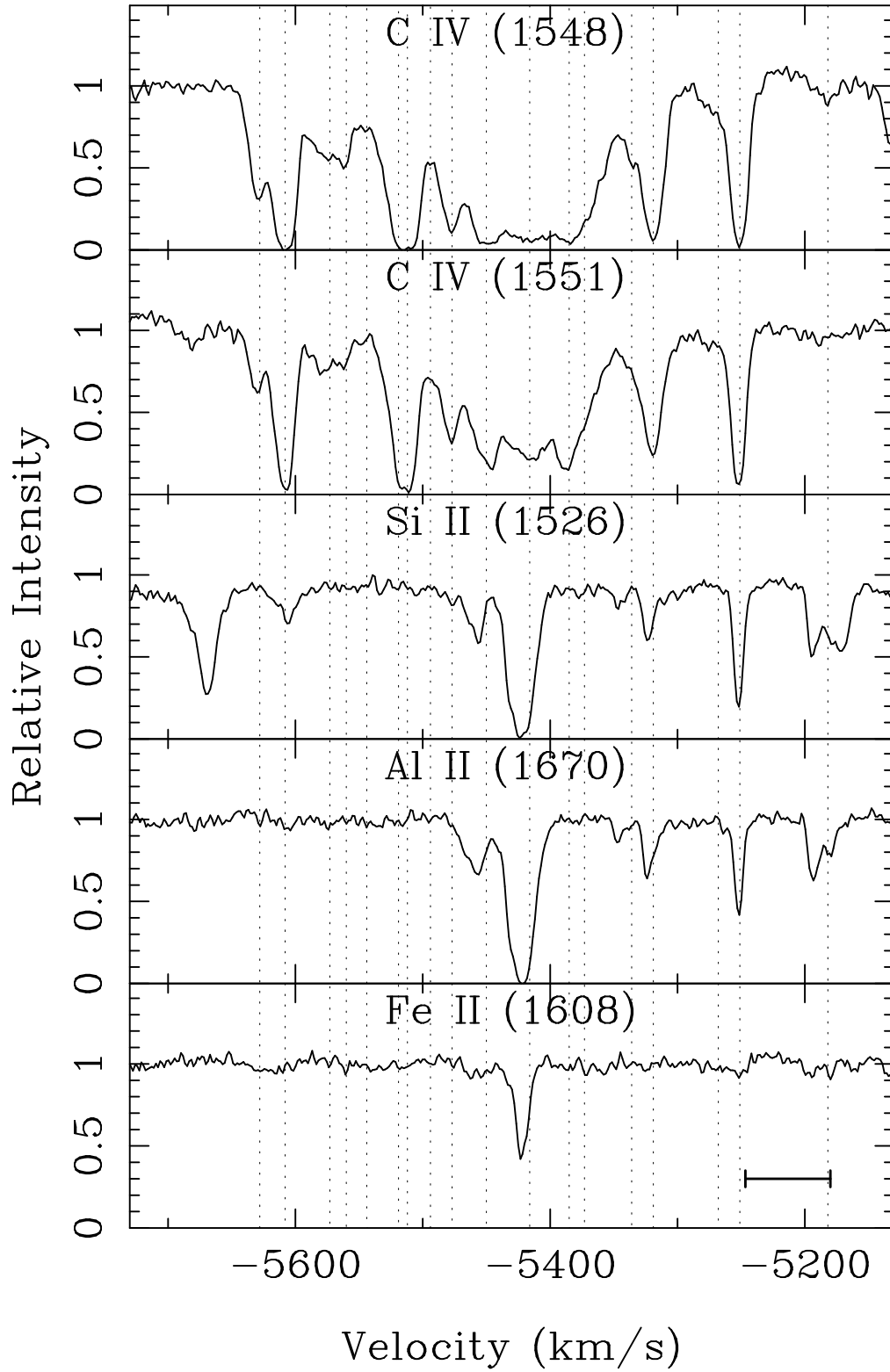


Fig. 5

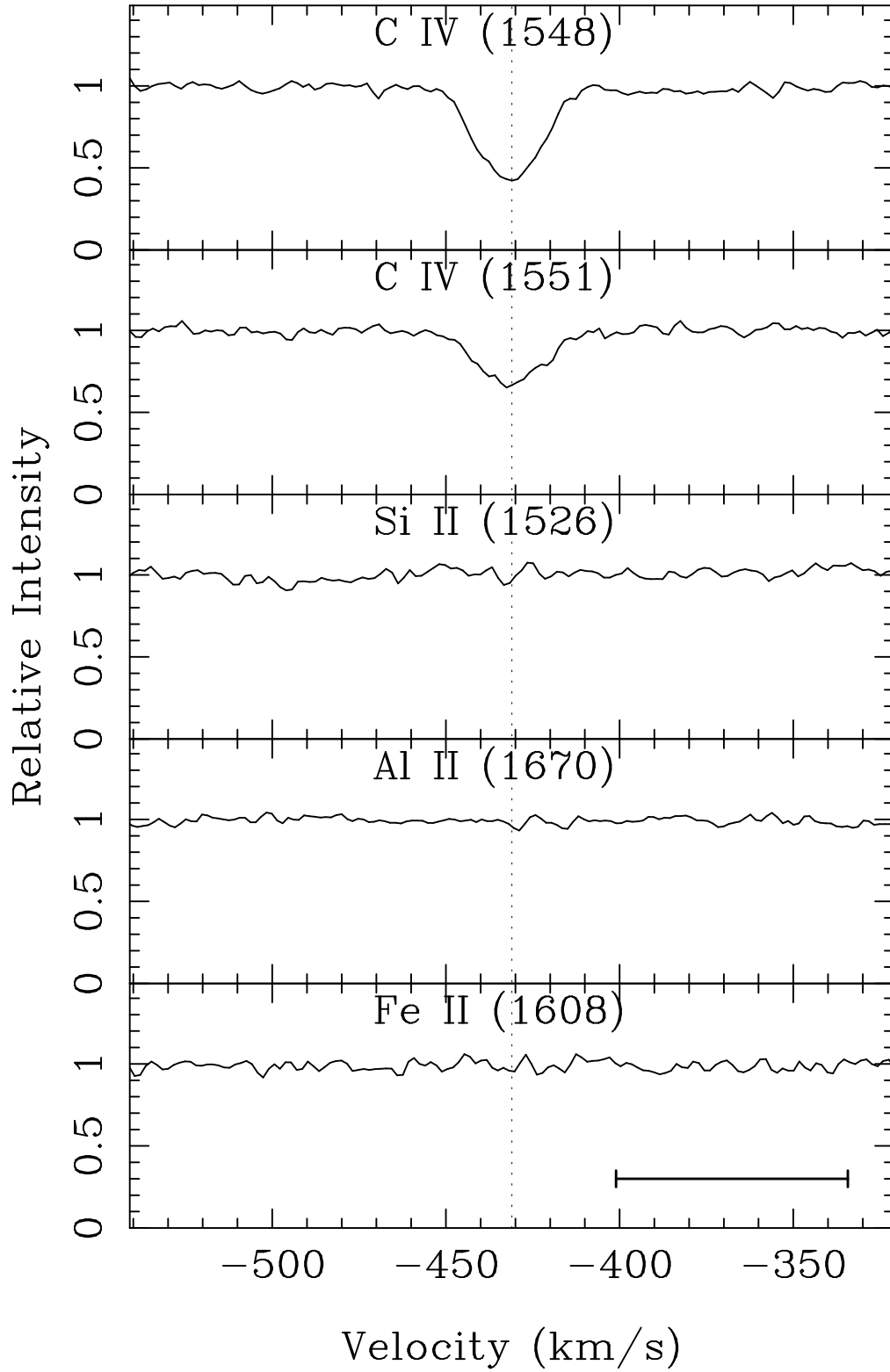


Fig. 6



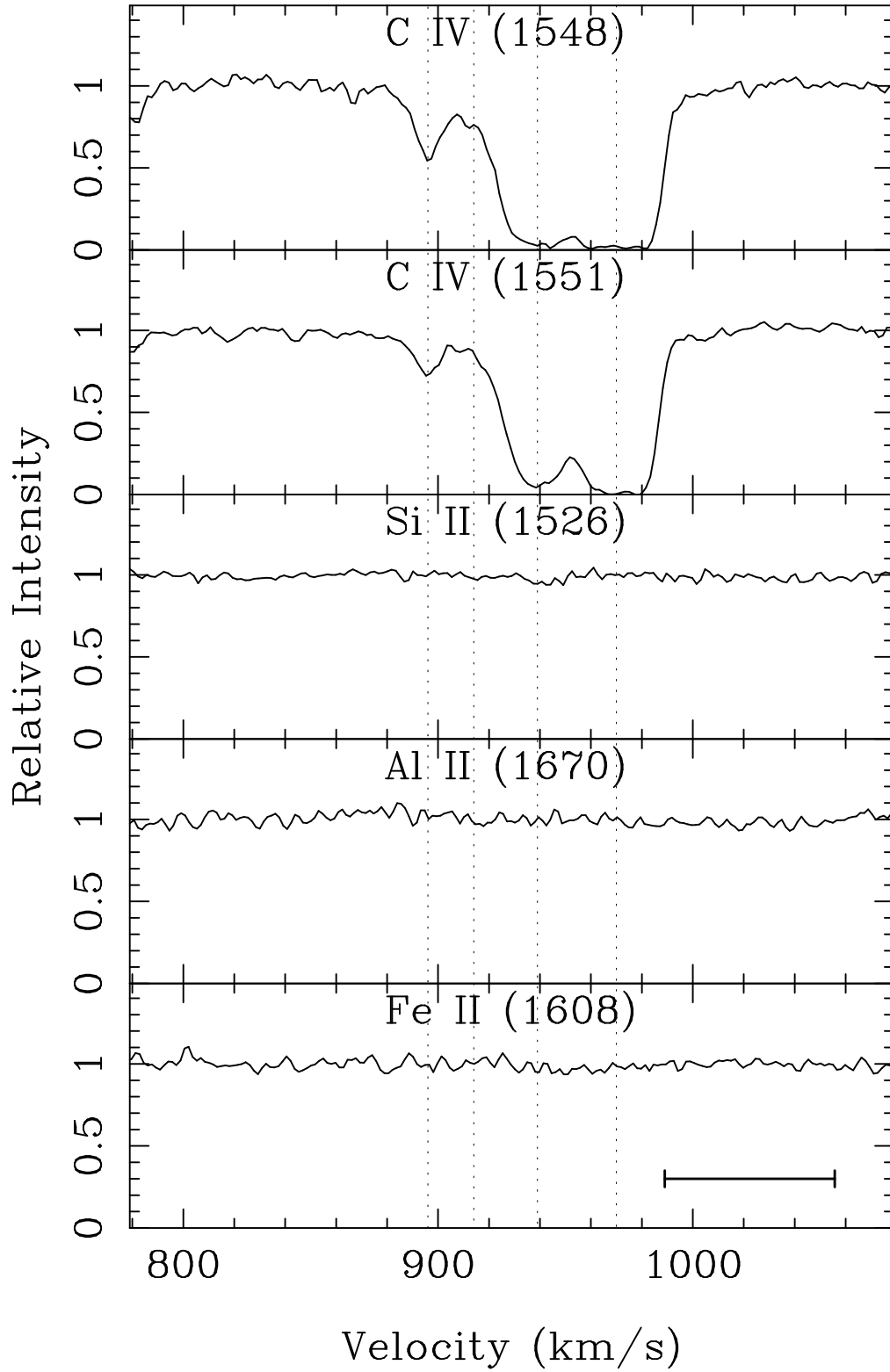


Fig. 7

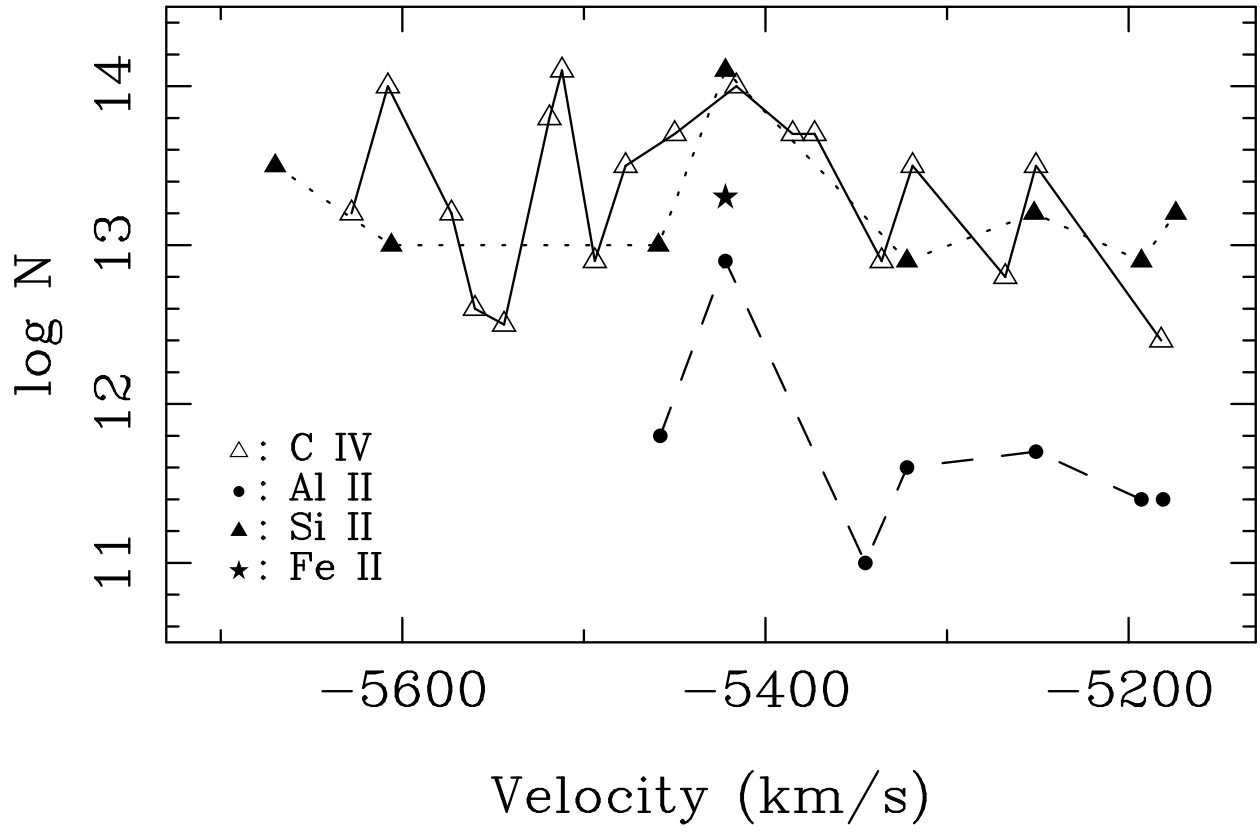


Fig. 8

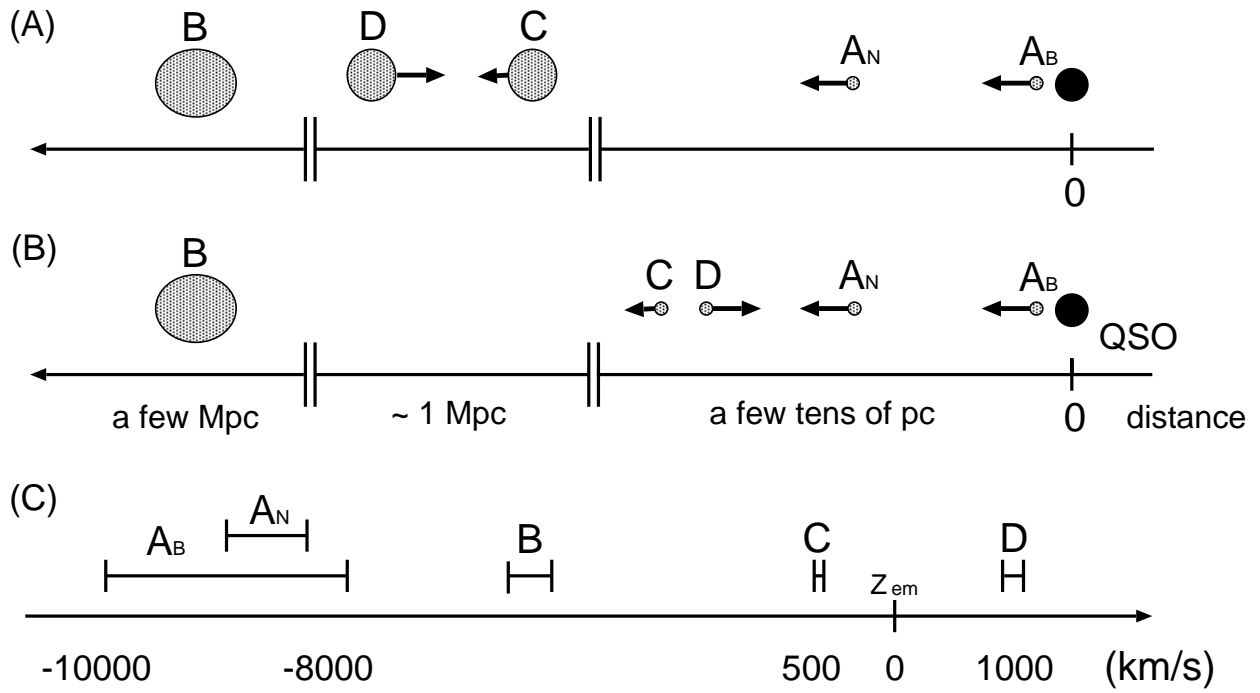


Fig. 9